Published in final edited form as:
Brain Res. 2013 August 21; 1527: . doi:10.1016/j.brainres.2013.06.012.

Correlated sodium and potassium imbalances within the ischemic core in experimental stroke: a ^{23}Na MRI and histochemical imaging study

Victor E. Yushmanov[a,*], **Alexander Kharlamov**[a], **Boris Yanovski**[a], **George LaVerde**[b,1], **Fernando E. Boada**[b,2], and **Stephen C. Jones**[a,b,c,d]

[a]Department of Anesthesiology, Allegheny-Singer Research Institute, Pittsburgh, PA 15212, USA

[b]MR Research Center, Department of Radiology, University of Pittsburgh School of Medicine, Pittsburgh, PA 15213, USA

[c]Department of Neurology, Allegheny-Singer Research Institute, Pittsburgh, PA 15212, USA

[d]Department of Biomedical Engineering, Carnegie-Mellon University, Pittsburgh, PA 15219, USA

Abstract

This study addresses the spatial relation between local Na^+ and K^+ imbalances in the ischemic core in a rat model of focal ischemic stroke. Quantitative [Na^+] and [K^+] brain maps were obtained by ^{23}Na MRI and histochemical K^+ staining, respectively, and calibrated by emission flame photometry of the micropunch brain samples. Stroke location was verified by diffusion MRI, by changes in tissue surface reflectivity and by immunohistochemistry with microtubule-associated protein 2 antibody. Na^+ and K^+ distribution within the ischemic core was inhomogeneous, with the maximum [Na^+] increase and [K^+] decrease typically observed in peripheral regions of the ischemic core. The pattern of the [K^+] decrease matched the maximum rate of [Na^+] increase ('slope'). Some residual mismatch between the sites of maximum Na^+ and K^+ imbalances was attributed to the different channels and pathways involved in transport of the two ions. A linear regression of the $[Na^+]_{br}$ vs. $[K^+]_{br}$ in the samples of ischemic brain indicates that for each K^+ equivalent leaving ischemic tissue, 0.8 ± 0.1 Eq, on average, of Na^+ enter the tissue. Better understanding of the mechanistic link between the Na^+ influx and K^+ egress would validate the ^{23}Na MRI slope as a candidate biomarker and a complementary tool for assessing ischemic damage and treatment planning.

Keywords

rat brain; focal ischemia; permanent MCAO; ^{23}Na MRI; tissue sodium; tissue potassium

[*]**Correspondence to:** Department of Anesthesiology, Allegheny-Singer Research Institute, 320 East North Avenue, Pittsburgh, PA 15212-4772, USA. Voice: 1-412-359-4362, Fax: 1-412-359-5288, vyushman@wpahs.org (V. E. Yushmanov).
[1]Present address: Department of Diagnostic Radiology, Yale University School of Medicine, New Haven, CT 06510, USA
[2]Present address: Department of Radiology, New York University Langone Medical Center, New York, NY 10016, USA

1. Introduction

Sodium and potassium in the brain are responsible for maintaining membrane potentials necessary for neuronal activity. In stroke, the supply of oxygen and glucose is not sufficient to power the Na/K ATPase, which provides active transport of these cations and thereby maintains their normal transmembrane concentration gradients. Depolarization and edema result in the equilibration of Na^+ and K^+ concentrations across the membranes, whereas the residual blood flow supports the influx or efflux routes for Na^+ and K^+. An increase in brain tissue sodium concentration ($[Na^+]_{br}$) after stroke, as well as a concomitant drop in potassium brain concentration ($[K^+]_{br}$), were well documented by brain sampling in animal models (Betz et al., 1994; Ito et al., 1979; Schuier and Hossmann, 1980; Shibata et al., 1974). Further refinement of brain sampling techniques enabled rapid measurements of $[Na^+]_{br}$ and $[K^+]_{br}$ locally even in small rodent brains (Yushmanov et al., 2007; Yushmanov et al., 2011). Recently, $[Na^+]_{br}$ has been considered as a potential biomarker for brain tissue viability after stroke (Boada et al., 2012; Thulborn et al., 1999), as well as a tool to determine the stroke onset time and establish patient eligibility for thrombolytic therapy (Jones et al., 2006). A change in $[K^+]_{br}$ has been suggested as an index of progressive ischemic damage, with possible connections to the integrity of the blood-brain barrier (BBB), developing vasogenic edema and post-ischemic hemorrhagic transformation (Jones et al., 2007; Yushmanov et al., 2009a), i.e., the events which are critical for success of thrombolytic therapy of stroke. Therefore, understanding of ion dynamics in the development of ischemic damage before reperfusion is essential for treatment planning. The question of the spatial relation between local Na^+ and K^+ imbalances, however, was never addressed; moreover, the analysis of brain tissue samples is not well-suited for this task.

Imaging-based approach presents clear advantages for mapping cation imbalances. ^{23}Na MRI has been validated as a quantitative technique to assess local $[Na^+]_{br}$ in the rat focal ischemia with 5-min time resolution using comparison of MRI-estimated $[Na^+]_{br}$ against emission flame photometry (Yushmanov et al., 2009c). ^{23}Na MRI timing of stroke is based upon the linear increase in $[Na^+]_{br}$ in affected areas in the first several hours (Wang et al., 2000; Yushmanov et al., 2007). To correlate MRI data with tissue pathology and biochemistry, high resolution three-dimensional (3D) histological data arrays must be accurately co-registered with MRI. Although for formalin-fixed and paraffin-embedded tissues the use of intermediate ex-vivo MRI and elastic registration may be required (Alic et al., 2011), a simple and efficient protocol is available for glass-mounted sections of the brain frozen inside the skull thus preserving its anatomic features (Yushmanov et al., 2009b; Yushmanov et al., 2009c). A reliable mapping of $[Na^+]_{br}$ increase in ischemia using ^{23}Na MRI with a small voxel size in small animal models enables the detailed characterization of regional inhomogeneities in brain sodium accumulation, whether between the ischemic core and potentially salvageable tissue (Wetterling et al., 2012) or within the ischemic core (Jones et al., 2006; Yushmanov et al., 2009b). Regional inhomogeneities in $[K^+]_{br}$ decrease in ischemic brain have been observed using histochemical staining (Kharlamov et al., 2007).

The purpose of this study was to test the hypothesis that the maximum decrease of $[K^+]_{br}$ and the maximum rate of $[Na^+]_{br}$ increase occur in the same peripheral regions of the ischemic core.

2. RESULTS

To meet the purpose of the study, a focal ischemic stroke was generated in rats. For quantitative comparison, $[Na^+]_{br}$ and $[K^+]_{br}$ maps were obtained by ^{23}Na MRI and histochemical K^+ staining, respectively, and calibrated by emission flame photometry of the micropunch brain samples. Histochemical staining provided higher spatial resolution and

more precise quantitation of $[K^+]_{br}$ (albeit only post mortem) in comparison with ^{87}Rb MRI (Yushmanov et al., 2011). Stroke presence and location was verified by MRI of the apparent diffusion coefficient (ADC), by changes in surface reflectivity of ischemic tissue, and by immunohistochemistry with microtubule-associated protein 2 (MAP2) antibody, as shown in Fig. 1

2.1. Physiological monitoring

Physiological variables at different phases of the experimental protocol were in the normal range for all animals, as summarized in Table 1. Minor fluctuations in physiological variables were not accompanied by changes in the ^{23}Na time courses.

2.2. $[Na^+]$ increase over the course of ischemia progression

The ischemic lesion (as defined by the ADC deficit, changes of surface reflectivity, and MAP2 staining) involved parts of the cortex and caudate putamen, as is typical for the suture middle cerebral artery occlusion (MCAO) model (Fig. 1). In 5 rats out of 8, the ^{23}Na MRI protocol was completed successfully, covering the time T_d after MCAO of 5.2 ± 0.5 h (mean ± SD). The site with a maximum rate of $[Na^+]_{br}$ increase ('slope') within the ischemic core was identified by ^{23}Na MRI as a 3D isocontour region of interest (ROI) at the 90% level of the maximum slope. A volume and position of the center of mass of the maximum slope ROI were determined using corresponding tools in AMIDE. In agreement with previously reported findings (Yushmanov et al., 2009b), $[Na^+]_{br}$ increase was inhomogeneous within the boundaries of the ischemic core (Figs. 1–3), the volume of the maximum slope ROI being 11 ± 7 mm^3 (mean ± SEM, n = 5); the numbers for individual animals are given in Table 2.

2.3. Local $[K^+]$ drop mirroring the $[Na^+]$ increase

K^+ staining revealed the inhomogeneity in $[K^+]_{br}$ distribution within the ischemic lesion in all animals. Of the five rats where the ^{23}Na MRI data were available, the pattern of the $[K^+]_{br}$ decrease matched the ROIs of maximum ^{23}Na slope (Figs. 2 and 3). To quantitatively characterize the relative locations of the maximum Na^+ increase and K^+ drop, the profiles of ^{23}Na slope and $[K^+]_{br}$ along the ribbons in the same coronal planes are shown below the corresponding images in Figs. 2 and 3e,f. The arched ribbons were placed so as to include the central and peripheral regions of the ischemic core and the "hot spots" of maximum ion imbalances. The maximum slope and maximum $[K^+]_{br}$ decrease were typically observed in peripheral regions of the ischemic core. Figure 3c,d presents an example (rat #5) where the lowest $[K^+]_{br}$ was found in the frontoparietal cortex at the dorsal edge of ischemic core (henceforth referred to as 'dorsal ischemic edge', region 1) and in the caudate putamen near the ventral edge of ischemic core ('ventral ischemic edge', region 3) as compared with the parietal cortex ('central ischemic core', region 2). Both regions 1 and 3 mirrored the regions of elevated ^{23}Na slope (Fig. 3a,b). A 3D reconstruction from 0.7-mm-separated K^+-stained coronal slices with the region defined by $[K^+]_{br} < 48 \pm 4$ mEq/kg shown in yellow indicates that the low-K^+ peripheral ischemic core completely surrounds the central ischemic core, and that its dorsal and rostral edges are narrower than the ventral and caudal ones (Fig. 3g). ROI of maximum ^{23}Na slope overlapped the low-K^+ ROI at both the dorsal and ventral ischemic edges. The values of $[Na^+]_{br}$ (extrapolated from ^{23}Na MRI data, as described elsewhere (Yushmanov et al., 2009c)) and $[K^+]_{br}$ in selected ROIs in the regions 1–3 and in control brain at the end of the experiment are given in Table 3 for this rat. It is apparent from the images and concentration estimates that at the rostral level, similar $[K^+]_{br}$ depletion at both dorsal (region 1) and ventral (region 3) edges was accompanied by approximately twice more significant increase in $[Na^+]_{br}$ at the ventral edge than at the dorsal edge. At the caudal level, in contrast, $[K^+]_{br}$ dropped and $[Na^+]_{br}$ peaked similarly at both edges.

2.4. The ratio of Na^+ influx and K^+ efflux in ischemic brain

Table 3 shows that for each ROI in the ischemic brain of the rat #5, $[K^+]_{br}$ decrease ($\Delta[K^+]_{br}$) is higher than $[Na^+]_{br}$ increase ($\Delta[Na^+]_{br}$) compared with the values for contralateral hemisphere, $\Delta[Na^+]_{br}/\Delta[K^+]_{br} = 0.6 \pm 0.1$. In all 8 animals, $[Na^+]_{br}$ and $[K^+]_{br}$ were determined in the micropunch samples of ischemic tissue by flame photometry, and the data were fit to the equation $[Na^+]_{br} = -0.8\ [K^+]_{br} + 120$ mEq/kg ($R^2 = 0.55$), as shown in Fig. 4. The values of $[Na^+]_{br}$ and $[K^+]_{br}$ in ischemic brain differed between individual animals, in part, because these values depend on the time T_d elapsed after MCAO, and T_d differed for all rats (Table 2).

3. DISCUSSION

The present study demonstrated that spatial correlation of ^{23}Na MRI and quantitative histochemical K^+ staining in 3D provides detailed insight into heterogeneity of ionic imbalances within the ischemic core in an animal model of permanent focal stroke by assessing dynamics of brain Na^+ and K^+ in the absence of reperfusion. A linear increase in $[Na^+]_{br}$ with evolution time of cerebral ischemia (between 1 and 6 h after MCAO) justifies the use of slope to pinpoint the site of the strongest disturbance of Na^+ metabolism (Boada et al., 2012; Jones et al., 2006; Thulborn et al., 1999; Wang et al., 2000; Yushmanov et al., 2007; Yushmanov et al., 2009b). The ROI of maximum ^{23}Na slope in the ischemic core (the core was defined by ADC, MAP2 and reflective changes) corresponds to the maximum decrease of $[K^+]_{br}$ in the same regions (Fig. 2 and Fig. 3, regions 1 and 3).

In agreement with earlier data for ^{23}Na slope (Yushmanov et al., 2009b), the sites of maximum $[Na^+]_{br}$ and $[K^+]_{br}$ imbalances within the ischemic core tended to be located at the core periphery (Figs. 2 and 3). The edge location of “hot spots” of cation imbalance is the argument in favor of the key role of residual or collateral circulation in the pathophysiology of ischemic stroke. Though energy depletion is a primary cause of ischemic brain edema, the resulting disturbances of water and ion homeostasis are mediated by residual trickle flow delivering more Na^+ and resulting in a more severe edema (Kato et al., 1987). The degree of imbalance between different edges of the ischemic core, however, is highly variable (Figs. 2 and 3); moreover, some edges may not develop excessive $[Na^+]_{br}$ increase or $[K^+]_{br}$ drop (relative to the central core) at all, as was also found in the rat stroke model using middle cerebral artery (MCA) transection with bilateral common carotid artery occlusion (MCAT) (Kharlamov et al., 2007).

The location of the maximum Na^+/K^+ imbalances supports the concept of the peripheral ischemic core as a region characterized by more prominent edema formation (Kato et al., 1987). The low-K^+ peripheral ischemic core, although associated with a progression of ischemic pathology, is not currently recognized as its inherent characteristic and a possible treatment target. Our current and recent findings discovered an array of critical events at the peripheral ischemic core after experimental focal ischemia. The drop of $[K^+]_{br}$ occurs in concert with the increase in $[Na^+]_{br}$ (Jones et al., 2006), peri-infarct depolarizations (Menon et al., 2012; Yushmanov et al., 2012), and the transient BBB disruption (as indicated by Gd-DTPA extravasation) at the peripheral ischemic core at 3–4 h after onset of experimental focal cerebral ischemia in the rat (Jones et al., 2007; Yushmanov et al., 2009a). In previous studies, a more severe decrease of $[K^+]_{br}$ at the edges of the ischemic region was reported in gerbils (Kato et al., 1987) and in the MCAT model in rats (Kharlamov et al., 2007). Expression of water channel aquaporin-4 was reported to increase in both the ischemic core and the ischemic border region, whereas that of aquaporin-3, -5 and -8 increased in the border region, even while decreasing in the ischemic core (Yang et al., 2009). Among other changes specific for the peripheral ischemic core are those of the immunoreactivities of MAP2 (Dawson and Hallenbeck, 1996; Kharlamov et al., 2001; Pettigrew et al., 1996) and

of the regulatory element, SUR1, of a non-specific cation channel, SUR1/TRPM4, a possible late mediator of Na^+-influx and K^+-efflux after 3 h of the hypoxic/ischemic conditions (Simard et al., 2012). Therefore, it may be argued that the Na^+/K^+ imbalances and BBB disruption are consistent with higher trickle blood flow to the infarct edges than to the center (of the order of 5–10 mL/100 g/min (Jones et al., 1989), i.e., still below the ischemic threshold), and that these imbalances may signal the initial onset and mark the initial position of the developing vasogenic edema, as well as modulate the severity of ischemic damage.

The close yet imperfect match between the sites of maximum $[Na^+]_{br}$ and $[K^+]_{br}$ imbalances (Fig. 3) may be attributed to the different channels and pathways involved in transport of the two ions. The likely route to explain K^+-efflux from the peripheral ischemic core is the paravascular route from the brain surface to the subarachnoid space mediated by aquaporin-4 (Iliff et al., 2012). In addition, endothelial K^+ and Na^+ channels/transporters provide the transcellular route across the BBB for these cations: e.g., Na^+ ions enter the brain via the luminal endothelial $Na^+/K^+/2Cl^-$ cotransporter (O'Donnell et al., 2004) and abluminal Na/K ATPase; K^+ efflux is via the same abluminal Na/K ATPase as well as an abluminal fraction of the $Na^+/K^+/2Cl^-$ cotransporter (the latter is 80%-luminal/20%-abluminal (O'Donnell et al., 2004)) and further by the luminal amiloride-sensitive Na^+-and K^+-selective channel (Vigne et al., 1989). It was suggested that increases in brain extracellular $[K^+]$ (such as those occurring in ischemic depolarization) may activate Na/K ATPase-mediated ion transport across the cerebral capillary, but will have little effect on Na/K ATPase activity in neurons (Schielke et al., 1990). Recent data have emphasized the role of activation of the $Na^+/K^+/2Cl^-$cotransporter (presumably, involving activation of AMP-kinase (Wallace et al., 2011)) and of a luminal Na^+/H^+ exchanger in cerebral edema formation in ischemic conditions (Luo et al., 2008; O'Donnell et al., 2004). The estimate of net relative fluxes of Na^+ vs. K^+ occurring via different mechanisms into and out of the ischemic brain (Fig. 4) indicates that for each K^+ equivalent leaving ischemic tissue, 0.8 ± 0.1 Eq, on average, of Na^+ enter the tissue, which is significantly different from the 1.5 ratio of Na^+ and K^+ cations transported by the Na/K ATPase.

In summary, ^{23}Na MRI and quantitative histochemical K^+ staining revealed heterogeneity in the rate of $[Na^+]_{br}$ increase, or slope, and in $[K^+]_{br}$ distribution within the ischemic core. Maximum changes in $[Na^+]_{br}$ and $[K^+]_{br}$, although their patterns are not identical, occur together at the periphery of ischemic core. This suggests the difference in pathophysiologic processes between the center and periphery of the infarct core and attests to the role of collateral circulation in the edge regions. Further refinement of the ion dynamics in peripheral ischemic core will take advantage of ^{87}Rb MRI in vivo for the study of the time course of $[K^+]_{br}$ in individual ischemic brain (Yushmanov et al., 2007; Yushmanov et al., 2011). Better understanding of the mechanistic link between the Na^+ influx and K^+ egress would validate the ^{23}Na MRI slope as a candidate biomarker and a complementary tool for assessing ischemic damage and treatment planning. More generally, the peripheral ischemic core requires particular attention for better understanding the mechanisms of ischemic pathology.

4. Experimental procedures

4.1. Animal preparation

Approval for animal use was obtained from the Allegheny-Singer Research Institute's Institutional Animal Care and Use Committee (IACUC) and was consistent with the "Guide for the Care and Use of Laboratory Animals" (Eighth Edition, 2011). Eight normally fed male Sprague-Dawley rats weighing 310 ± 30 g (mean ± SD) were used. Anesthesia was induced with 3% and maintained with 1.0% isoflurane (up to 2.5% when needed), 30%

oxygen, and balance nitrous oxide, administered via endotracheal tube and artificial respiration (Model 681, Harvard Apparatus, South Natick, MA, USA). Femoral arterial and venous catheters were inserted. Inside the magnet, a MR compatible ventilator (MRI-1, CWE, Ardmore, PA, USA) was used. Arterial blood pressure was continuously monitored from a femoral artery using a strain gauge transducer (DT-XX, Viggo Spectramed, Miami, FL, USA) and recorded on a polygraph (Gould, Cleveland, OH, USA). An appropriate maintenance level of isoflurane was determined by monitoring the blood pressure response to tail pinch. Body temperature was maintained at 37°C by a servocontrolled system consisting of a rectal temperature probe and a heating blanket outside the magnet or a thermostated water jacket inside the magnet. Immobilization was implemented with 0.4 mg/kg pancuronium bromide injected intramuscularly at 60 min intervals (on the bench) or continuously infused intravenously at 0.4 mg/kg/h (delivered at 1 mL/h) inside the magnet. To ensure physiological stability, arterial blood pH and gases ($PaCO_2$, PaO_2) were measured (ABL-3, Radiometer America, Westlake, OH, USA) before surgery, at different phases of surgery, and at regular intervals during MRI; in total, typically, at 4–7 time points. With the blood volume per sample being of ≈ 65 μL, the total volume of withdrawn blood was not hemodynamically significant.

4.2. Occlusion of the middle cerebral artery

In seven animals, permanent focal cerebral ischemia was produced by insertion of an intraluminal suture. The 3–0 monofilament poly-L-lysine coated nylon suture was inserted 20–21 mm through the internal carotid artery and further into the circle of Willis, occluding the MCA at its origin (Belayev et al., 1996). In one animal, MCAT was performed as described previously (Jones et al., 2006; Wang et al., 2000).

4.3. MRI

For $^{23}Na/^{1}H$ MRI, the animal's head was positioned inside a 5-cm-diameter, 5-cm-long dual-tuned dual-quadrature birdcage transmit/receive radiofrequency (RF) coil (Shen et al., 1997) in the animal cradle with a recirculating water bed and fittings for respiratory and anesthesia gas supply. Images were obtained on a 3 T whole body scanner (GE Healthcare, Waukesha, WI, USA) within a field of view of 50×50×50 mm as described elsewhere (Yushmanov et al., 2009b; Yushmanov et al., 2009c). ^{1}H diffusion-weighted multislice spin-echo images (*TR/TE* of 2000/140 ms, in-plane resolution of 0.2 mm, eight 3.2-mm-thick slices, diffusion weighting *b*-factor values of 0, 93, 372, and 837 s/mm^2, scan time of 4.7 min per *b*-factor), with the diffusion-sensitizing gradient applied along each of the Cartesian axes, were used for reconstruction of ADC trace maps. ^{23}Na MRI was performed using a 3D twisted projection imaging scheme (Boada et al., 1997b) with a voxel size of 0.48 mm^3, imaging time of 5.3 min (eight transients for each of 398 projections), and the inhomogeneity correction of the B_1 field by RF mapping (Boada et al., 1997a; Yushmanov et al., 2009c). An ultra-short *TE* of 0.4 ms and a long *TR* of 100 ms were used to eliminate a quantitation bias resulting from possible changes in relaxation times T_1 and T_2 in ischemic brain. Cylindrical tubes containing NaCl solutions at different concentrations (0, 77, 116 and 154 mM) were placed next to animal's head and served as external position and concentration references after correction for partial ^{23}Na signal saturation in the solution due to its longer T_1 (T_1 = 60 ms, correction factor $1 - \exp(-TR/T_1)$). Tissue ^{23}Na with T_1 of 10–30 ms is fully relaxed in these conditions. The ^{23}Na MRI series typically spanned two to four hours within a 1- to 6-hour window after ischemia.

4.4. Brain processing

After the end of MRI scanning (typically, 4.5 to 6 h after MCAO), rats were decapitated, and their heads were immediately frozen in dry ice and stored at −80°C in order to preserve

the spatial characteristics of the brain for further superposition and comparison with MR images. The brain was chipped out of the skull in a −20°C cold box and mounted into the cryostat (−8°C). Twelve to 18 samples of approximately 0.5 mg wet weight were punched from the ipsilateral and contralateral brain (Yushmanov et al., 2007; Yushmanov et al., 2009c) at two or three coronal levels, typically between +1 and −4 mm from bregma. The micro-puncher inner diameter was 0.53 mm, the sampling depth was determined by examining coronal brain cuts taken every 35-μm, and the samples were precision-weighed using a Cahn model C-44 microbalance (ATI Orion, Boston, MA, USA). The sampling location was guided by ADC and ^{23}Na maps of the brain (Yushmanov et al., 2009b) and by the change in surface reflectivity of ischemic tissue (Kharlamov et al., 2001), as shown in Fig. 1a,b,d. Cut-face photographs of the brain were taken at several levels (Fig. 1c), including punched surfaces before and after sampling (Yushmanov et al., 2009b). The 35-μm thick coronal sections of the brain at different levels from bregma were mounted on glass slides and digitized. The infarct size and location were verified by reflective changes and by immunohistochemistry with MAP2 antibody in slide-mounted brain sections (Kharlamov et al., 2001), as shown in Fig. 1d,f. Na and K content in punched samples was determined by emission flame photometry at 589 and 766 nm, respectively, using an IL943 flame photometer (Instrumentation Laboratory, Lexington, MA, U.S.A.). The spatial distribution of $[K^+]_{br}$ in unfixed slide-mounted coronal brain sections was determined by histochemical potassium staining (Kharlamov et al., 2007; Mies et al., 1984). Batches of up to 25 sections were placed in a section holder to assure equivalent timing (for each batch) during processing. Sections were: 1) incubated in sodium cobaltinitrite solution for 2 min; 2) quickly washed in distilled water (3 × 10 sec); 3) dehydrated in 96% ethyl alcohol for 30 sec; 4) incubated in ammonium sulfide/ethyl alcohol (50/50) for 30 sec; 5) dehydrated in absolute ethyl alcohol for 1 min; 6) cleaned in xylene for 5 min; 7) immediately cover-slipped with Permount. All procedures were performed in a 4°C-cold room, and all solutions were kept at 1–2°C. All sections of the same brain were stained in the same batch; sections of different brains were stained in separate batches.

4.5. Image processing

Parametric ^{1}H ADC maps were generated pixel-wise by exponential fitting of the diffusionweighted image intensity vs. the *b* value (Le Bihan et al., 1986) in MATLAB (MathWorks, Natick, MA, USA). ^{23}Na MR images were reconstructed, corrected for inhomogeneity of the B_1 field and for the non-zero noise baseline in the magnitude mode reconstruction (Boada et al., 1997a), stacked in four dimensions (including the time dimension), and parametric images of the rate of ^{23}Na signal increase ('slope') were generated from the serial ^{23}Na images (by performing a pixel-wise linear regression of image intensity versus time after stroke onset) using C and C++ scripts in the UNIX environment. Selected 35-μm-thick coronal brain slices (taken every 350 μm) and histological MAP2 and K^+-stained sections (taken every 700 μm) were digitized, stacked and co-registered using ImageJ (Schneider et al., 2012) to render volumetric reconstructions of the sampled brain. MR images were aligned with histological 3D images and cut-face photographs and analyzed using the AMIDE software (Loening and Gambhir, 2003). The $[Na^+]_{br}$ values were obtained after MRI calibration against flame photometry as described elsewhere (Yushmanov et al., 2009c) by placing cylindrical ROIs in the ^{23}Na images at the positions of punch voids on histological and cut-face images, as shown in Fig. 1. To generate quantitative $[K^+]_{br}$ maps, image intensity in the histochemically stained images was 1) corrected for minor staining variations by assuming the stable $[K^+]_{br}$ (and, hence, constant optical density) in the normal cortex, and 2) calibrated against $[K^+]$ obtained by flame photometry (Kharlamov et al., 2007) (Figs. 1e, 5 and Table 2). For each punch sample, the average of K^+ image intensities at both ends of the sample was used for calibration. Individual calibrations were performed for each animal separately because of the

variations of staining intensity between the batches. The calibrated 2D images of $[K^+]_{br}$ and ^{23}Na slope were then redigitized to 207×207 pixels and co-analyzed for spatial changes using the 'ribbon' tool of the MCID imaging system (InterFocus Imaging Ltd., Linton, UK). $[K^+]_{br}$ and slope profiles along the ribbon were smoothed using a 15-point moving average or a 10-point FFT filter, respectively (OriginPro 8.1 SR1, OriginLab Corp., Northampton, MA, USA).

4.6. Statistics

Two-tailed analysis of variance was applied for significance of differences, independent or paired as appropriate, with a post hoc Bonferroni correction when multiple comparisons were made, using SPSS for Windows, version 14.0 (SPSS, Chicago, IL, USA). $P < 0.05$ was taken as indicating significance. The errors are presented as SD or SEM, as indicated. Linear regressions were performed, and correlation coefficients and 95% confidence limits were calculated.

Acknowledgments

This work was supported by NIH grants NS30839 and NS66292. We are grateful for the technical assistance provided by Ms. Jayjayantee Dasgupta

Abbreviations

3D	three-dimensional
ADC	apparent diffusion coefficient
BBB	blood-brain barrier
MAP2	microtubule-associated protein 2
MCA, MCAO, MCAT	middle cerebral artery, MCA occlusion, and MCA transection with bilateral common carotid artery occlusion, respectively
$[Na^+]_{br}$ and $[K^+]_{br}$	brain tissue sodium and potassium concentration, respectively
RF	radiofrequency
ROI	region of interest

REFERENCES

Alic L, Haeck JC, Bol K, Klein S, van Tiel ST, Wielepolski PA, de JM, Niessen WJ, Bernsen M, Veenland JF. Facilitating tumor functional assessment by spatially relating 3D tumor histology and in vivo MRI: image registration approach. PLoS ONE. 2011; 6:e22835. [PubMed: 21897840]

Belayev L, Alonso OF, Busto R, Zhao W, Ginsberg MD. Middle cerebral artery occlusion in the rat by intraluminal suture. Neurological and pathological evaluation of an improved model. Stroke. 1996; 27:1616–1622. [PubMed: 8784138]

Betz AL, Keep RF, Beer ME, Ren X. Blood-brain barrier permeability and brain concentration of sodium, potassium, and chloride during focal ischemia. J. Cereb. Blood Flow Metab. 1994; 14:29–37. [PubMed: 8263055]

Boada FE, Gillen JS, Noll DC, Shen GX, Chang SY, Thulborn KR. Data acquisition and postprocessing strategies for fast quantitative sodium imaging. Int. J. Imaging Syst. Technol. 1997a; 8:544–550.

Boada FE, Gillen JS, Shen GX, Chang SY, Thulborn KR. Fast three dimensional sodium imaging. Magn. Reson. Med. 1997b; 37:706–715. [PubMed: 9126944]

Boada FE, Qian Y, Nemoto E, Jovin T, Jungreis C, Jones SC, Weimar W, Lee V. Sodium MRI and the assessment of irreversible tissue damage during hyper-acute stroke. Transl. Stroke Res. 2012; 3:236–245. [PubMed: 24323779]

Dawson DA, Hallenbeck JM. Acute focal ischemia-induced alterations in MAP2 immunostaining: description of temporal changes and utilization as a marker for volumetric assessment of acute brain injury. J. Cereb. Blood Flow Metab. 1996; 16:170–174. [PubMed: 8530550]

Iliff JJ, Wang M, Liao Y, Plogg BA, Peng W, Gundersen GA, Benveniste H, Vates GE, Deane R, Goldman SA, Nagelhus EA, Nedergaard M. A paravascular pathway facilitates CSF flow through the brain parenchyma and the clearance of interstitial solutes, including amyloid beta. Sci. Transl. Med. 2012; 4 147ra111.

Ito U, Ohno K, Nakamura R, Suganuma F, Inaba Y. Brain edema during ischemia and after restoration of blood flow: measurement of water, sodium, potassium content and plasma protein permeability. Stroke. 1979; 10:542–547. [PubMed: 505496]

Jones SC, Bose B, Furlan AJ, Friel HT, Easley KA, Meredith MP, Little JR. CO_2 reactivity and heterogeneity of cerebral blood flow in ischemic, border zone, and normal cortex. Am. J. Physiol. Heart Circ. Physiol. 1989; 257:H473–H482.

Jones SC, Hu W, Wang Y, Perez-Trepichio AD, Yushmanov VE, Kharlamov A, Boada FE. Stability and abrupt fall of brain tissue potassium in rat focal cerebral ischemia and the blood-brain barrier. J. Cereb. Blood Flow Metab. 2007; 27(suppl S1):BO05–BO09.

Jones SC, Kharlamov A, Yanovski B, Kim DK, Easley KA, Yushmanov VE, Ziolko SK, Boada FE. Stroke onset time using sodium MRI in rat focal cerebral ischemia. Stroke. 2006; 37:883–888. [PubMed: 16424376]

Kato H, Kogure K, Sakamoto N, Watanabe T. Greater disturbance of water and ion homeostasis in the periphery of experimental focal cerebral ischemia. Exp. Neurol. 1987; 96:118–126. [PubMed: 3556505]

Kharlamov A, Kim DK, Jones SC. Early visual changes in reflected light on non-stained brain sections after focal ischemia mirror the area of ischemic damage. J. Neurosci. Methods. 2001; 111:67–73. [PubMed: 11574121]

Kharlamov A, Yushmanov VE, Jones SC. Prominent decrease of brain tissue K^+, $[K^+]_{br}$, in the peripheral regions of ischemic core evaluated by quantitative histological potassium staining. J. Cereb. Blood Flow Metab. 2007; 27(suppl S1) BP53-07W.

Le Bihan D, Breton E, Lallemand D, Grenier P, Cabanis E, Laval-Jeantet M. MR imaging of intravoxel incoherent motions: application to diffusion and perfusion in neurologic disorders. Radiology. 1986; 161:401–407. [PubMed: 3763909]

Loening AM, Gambhir SS. AMIDE: a free software tool for multimodality medical image analysis. Mol. Imaging. 2003; 2:131–137. [PubMed: 14649056]

Luo J, Wang Y, Chen H, Kintner DB, Cramer SW, Gerdts JK, Chen X, Shull GE, Philipson KD, Sun D. A concerted role of Na^+ -K^+ -Cl^- cotransporter and Na^+/Ca^{2+} exchanger in ischemic damage. J. Cereb. Blood Flow Metab. 2008; 28:737–746. [PubMed: 17912271]

Menon, PG.; Kharlamov, A.; Yushmanov, VE.; Yutzy, SR.; Schornack, PA.; Wiener, EC.; Boada, FE.; Jones, SC. Neuroscience Meeting Planner, Neuroscience. New Orleans, LA: 2012 Oct 13–17. Automatic spatial identification and 4D tracking of peri-infarct depolarizations in ischemic rat brain using fast ADC MRI. Program#506.24.

Mies G, Kloiber O, Drewes LR, Hossmann KA. Cerebral blood flow and regional potassium distribution during focal ischemia of gerbil brain. Ann. Neurol. 1984; 16:232–237. [PubMed: 6476795]

O'Donnell ME, Tran L, Lam TI, Liu XB, Anderson SE. Bumetanide inhibition of the blood-brain barrier Na-K-Cl cotransporter reduces edema formation in the rat middle cerebral artery occlusion model of stroke. J. Cereb. Blood Flow Metab. 2004; 24:1046–1056. [PubMed: 15356425]

Pettigrew LC, Holtz ML, Craddock SD, Minger SL, Hall N, Geddes JW. Microtubular proteolysis in focal cerebral ischemia. J. Cereb. Blood Flow Metab. 1996; 16:1189–1202. [PubMed: 8898691]

Schielke GP, Moises HC, Betz AL. Potassium activation of the Na,K-pump in isolated brain microvessels and synaptosomes. Brain Res. 1990; 524:291–296. [PubMed: 1963338]

Schneider CA, Rasband WS, Eliceiri KW. NIH Image to ImageJ: 25 years of image analysis. Nat. Methods. 2012; 9:671–675. [PubMed: 22930834]

Schuier FJ, Hossmann KA. Experimental brain infarcts in cats. II. Ischemic brain edema. Stroke. 1980; 11:593–601. [PubMed: 7210064]

Shen GX, Boada FE, Thulborn KR. Dual-frequency, dual-quadrature, birdcage RF coil design with identical B_1 pattern for sodium and proton imaging of the human brain at 1.5 T. Magn Reson. Med. 1997; 38:717–725. [PubMed: 9358445]

Shibata S, Hodge CP, Pappius HM. Effect of experimental ischemia on cerebral water and electrolytes. J. Neurosurg. 1974; 41:146–159. [PubMed: 4841873]

Simard JM, Woo SK, Schwartzbauer GT, Gerzanich V. Sulfonylurea receptor 1 in central nervous system injury: a focused review. J. Cereb. Blood Flow Metab. 2012; 32:1699–1717. [PubMed: 22714048]

Thulborn KR, Gindin TS, Davis D, Erb P. Comprehensive MRI protocol for stroke management: tissue sodium concentration as a measure of tissue viability in non-human primate studies and in clinical studies. Radiology. 1999; 213:156–166. [PubMed: 10540656]

Vigne P, Champigny G, Marsault R, Barbry P, Frelin C, Lazdunski M. A new type of amiloride-sensitive cationic channel in endothelial cells of brain microvessels. J. Biol. Chem. 1989; 264:7663–7668. [PubMed: 2468671]

Wallace BK, Foroutan S, O'Donnell ME. Ischemia-induced stimulation of Na-K-Cl cotransport in cerebral microvascular endothelial cells involves AMP kinase. Am. J. Physiol. Cell Physiol. 2011; 301:C316–C326. [PubMed: 21562306]

Wang Y, Hu W, Perez-Trepichio AD, Ng TC, Furlan AJ, Majors AW, Jones SC. Brain tissue sodium is a ticking clock telling time after arterial occlusion in rat focal cerebral ischemia. Stroke. 2000; 31:1386–1392. [PubMed: 10835461]

Wetterling F, Gallagher L, Macrae IM, Junge S, Fagan AJ. Regional and temporal variations in tissue sodium concentration during the acute stroke phase. Magn. Reson. Med. 2012; 67:740–749. [PubMed: 21678490]

Yang M, Gao F, Liu H, Yu WH, Sun SQ. Temporal changes in expression of aquaporin-3,-4,-5 and -8 in rat brains after permanent focal cerebral ischemia. Brain Res. 2009; 1290:121–132. [PubMed: 19616516]

Yushmanov VE, Kharlamov A, Boada FE, Jones SC. Monitoring of brain potassium with rubidium flame photometry and MRI. Magn. Reson. Med. 2007; 57:494–500. [PubMed: 17326173]

Yushmanov VE, Kharlamov A, Boada FE, Jones SC. Transient blood-brain barrier disruption and changes in brain electrolytes at the edge of the ischemic core. Proc. Intl. Soc. Mag. Reson. Med. 2009a; 17:3280.

Yushmanov VE, Kharlamov A, Ibrahim TS, Zhao T, Boada FE, Jones SC. K^+ dynamics in ischemic rat brain in vivo by ^{87}Rb MRI at 7 T. NMR Biomed. 2011; 24:778–783. [PubMed: 21834001]

Yushmanov VE, Kharlamov A, Yanovski B, LaVerde G, Boada FE, Jones SC. Inhomogeneous sodium accumulation in the ischemic core in rat focal cerebral ischemia by ^{23}Na MRI. J. Magn. Reson. Imaging. 2009b; 30:18–24. [PubMed: 19557842]

Yushmanov VE, Kharlamov A, Yutzy SR, Schornack PA, Menon PG, Wiener EC, Boada FE, Jones SC. 3D tracking of transient peri-infarct depolarizations in ischemic rat brain by fast ADC mapping. Proc. Intl. Soc. Mag. Reson. Med. 2012; 20:3063.

Yushmanov VE, Yanovski B, Kharlamov A, LaVerde G, Boada FE, Jones SC. Sodium mapping in focal cerebral ischemia in the rat by quantitative ^{23}Na MRI. J. Magn. Reson. Imaging. 2009c; 29:962–966. [PubMed: 19306443]

Highlights

- Spatial match between Na^+ and K^+ imbalances was observed in focal ischemic stroke.
- Na^+ and K^+ were mapped quantitatively by ^{23}Na MRI and histochemical K^+ staining.
- Residual Na^+/K^+ mismatch is due to their different transport mechanisms.
- The ratio of net fluxes of Na^+ vs. K^+ into and out of the ischemic brain is 0.8.
- ^{23}Na MRI could provide a candidate biomarker for stroke treatment planning.

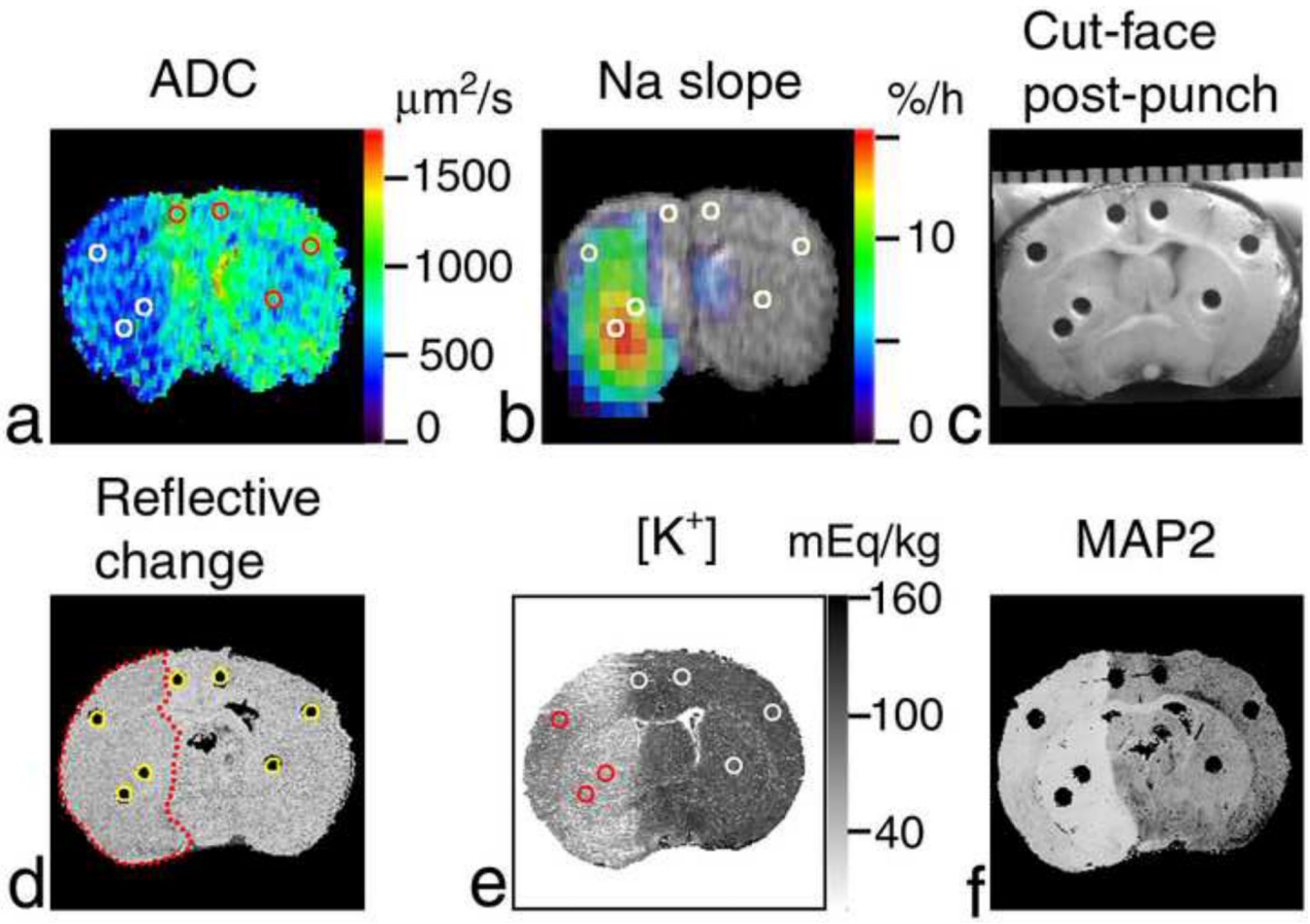

Figure 1.

Region-of-interest (ROI) analysis of Na^+ accumulation and K^+ drop in a rat brain after MCAO. Coronal images of the brain (at approximately bregma −0.4 mm) of the rat #5 are shown. (**a**) ADC map where ADC < 500 $\mu m^2/s$ in the ischemic area (left-hand side of the image). (**b**) Pseudocolor-coded parametric image of the rate of ^{23}Na signal increase ('slope') superimposed over the grayscale ^1H spin-echo MR image as an anatomic reference. Reference tubes with NaCl solutions were external to the rat head in the magnet and are not shown in MR images. (**c**) Cut-face photograph of the brain in the cryostat after sampling showing punch holes. A millimeter scale is shown at the top. Punch samples were analyzed using emission flame photometry. (**d**) Cross-section of the 3D reconstruction of the brain from the 35-μm-thick slices cut at 4.4 h after MCAO. The change in surface reflectivity of ischemic tissue shows the infarct location (outlined by a red dotted line). Cylindrical ROIs (yellow circles) were placed over the punch holes and are shown in images (a, b and e) as white or colored circles. (**e**) K^+-stained slice taken at the sampling plane and used to calibrate optical density against $[K^+]$. (**f**) The absence of staining in the MAP2-stained slice (separated by 0.67 mm from the sampling plane) indicates the ischemic lesion.

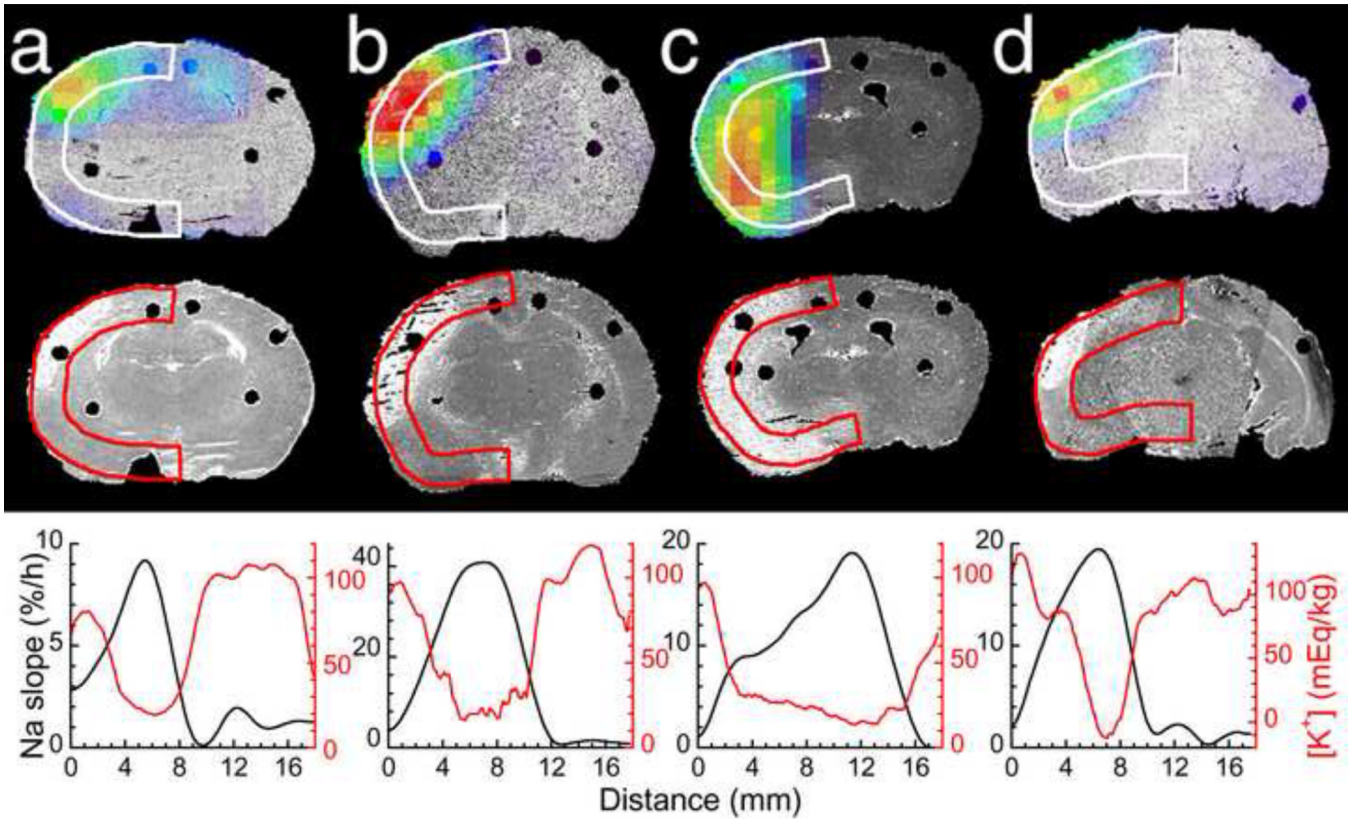

Figure 2.

Spatial match of Na^+ accumulation and K^+ drop in a rat brain after MCAO. (**a–d**) Coronal images of the brain of rats #2–4 and 6, respectively. Top row: pseudocolor-coded parametric image of the rate of ^{23}Na signal increase ('slope') superimposed over the grayscale 3D brain reconstructions from histological 35-μm-thick sections. Middle row: the same planes of 3D brain reconstructions from the K^+-stained sections. Lack of staining (white areas) indicate low $[K^+]_{br}$ in the ischemic lesion. Bottom row: ^{23}Na slope (black) and $[K^+]_{br}$ (red) profiles along the ribbons in the ischemic hemisphere (white or color arcs in the images) in the dorsal-to-ventral direction. Black dots in the images show holes in the brain after taking punch samples for calibration of Na^+ and K^+ images.

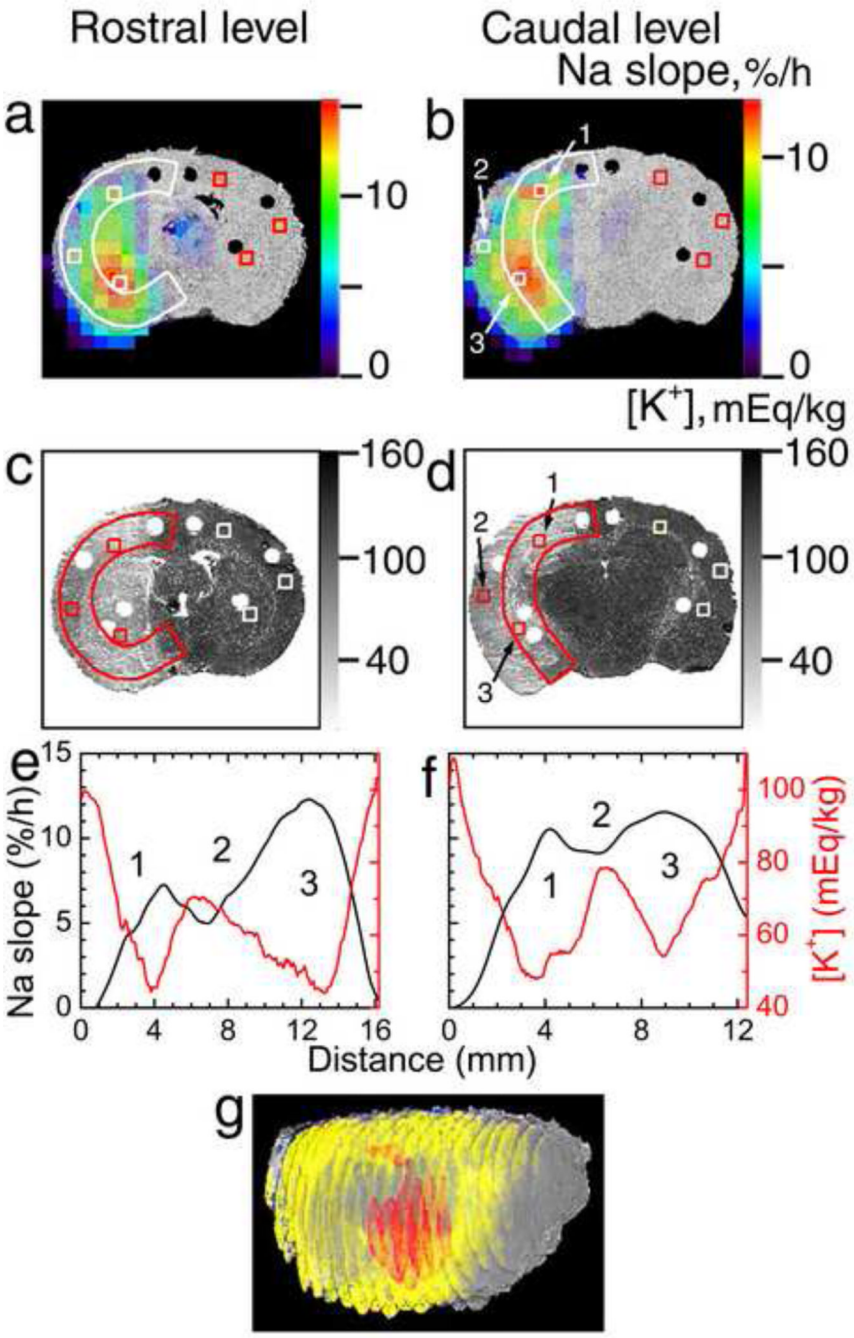

Figure 3.

Na^+ and K^+ mapping of the ischemic brain (rat #5). (**a,b**) Pseudocolor images of the ^{23}Na slope superimposed over the grayscale 3D reconstruction of the brain from histological 35-μm-thick sections. (**c,d**) K^+-stained slices cut at 4.4 h post MCAO. (**e,f**) ^{23}Na slope (black) and $[K^+]_{br}$ (red) profiles along the ribbons in the ischemic hemisphere (white or color arcs in (a)–(d)) in the dorsal-to-ventral direction. The coronal sections were taken at the rostral (bregma −0.4 mm, a,c,e) and caudal (bregma −3 mm, b,d,f) levels. (1) Dorsal ischemic edge; (2) central ischemic core; (3) ventral ischemic edge. Estimated $[Na^+]$ and $[K^+]$ in ipsilateral and homotopic contralateral ROIs (white or color squares in (a)–(d)) in regions 1–3 are

given in Table 3. (**g**) 3D reconstruction of the brain from 21 co-registered K^+-stained coronal slices (0.7-mm separation) as viewed from the front-right perspective. Regions with $[K^+]_{br}$ below 48 ± 4 mEq/kg (based on Gaussian-filtered images, to improve low-K^+ ROI contiguity) are shown in yellow to highlight the peripheral ischemic core surrounding the central ischemic core. ROI of maximum ^{23}Na slope corresponding to the slope range of 11.4 to 15.6%/h and overlapping the low-K^+ ROI is shown in red.

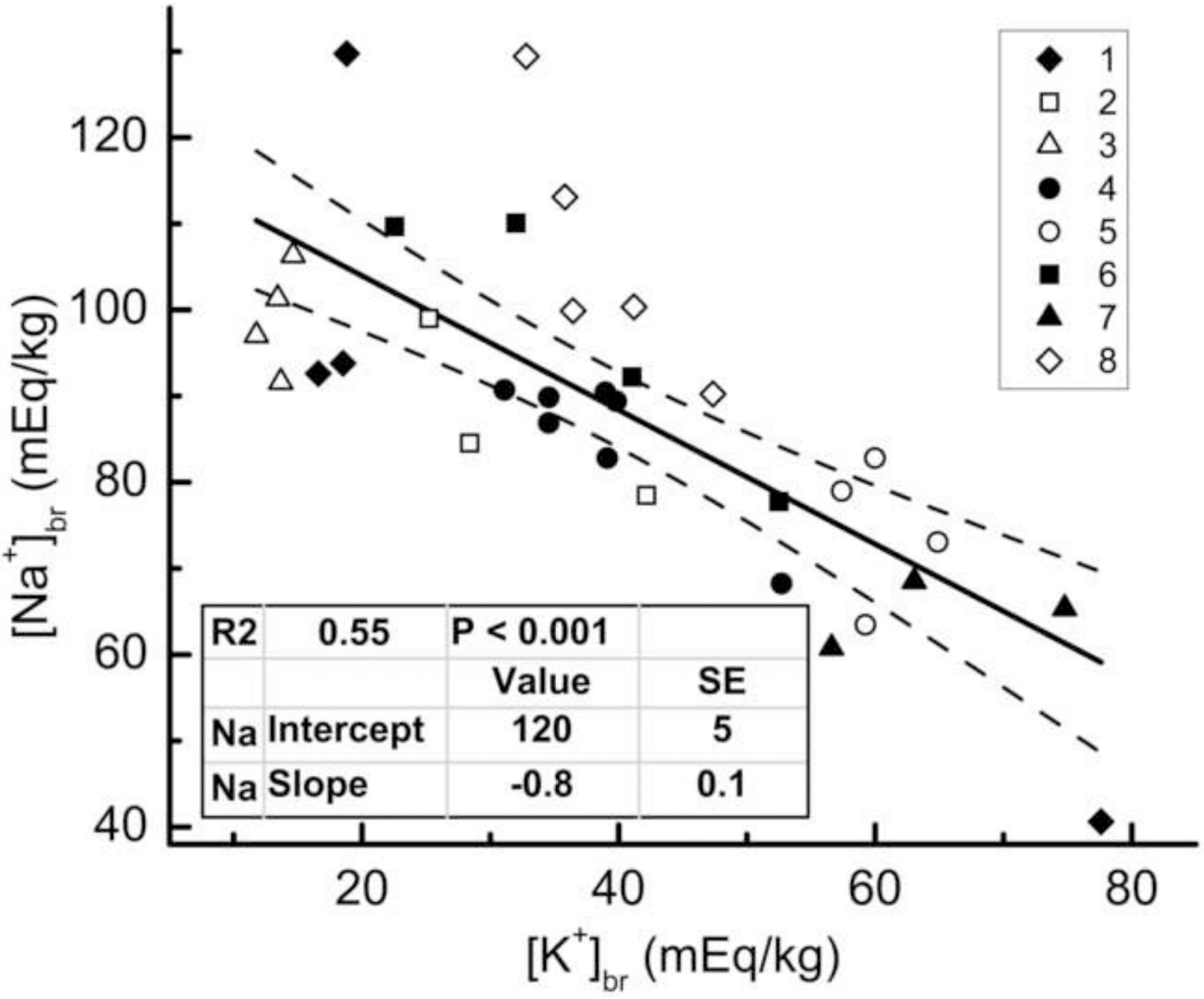

Figure 4.

Linear fit of $[Na^+]_{br}$ vs. $[K^+]_{br}$ in ischemic tissue. $[Na^+]_{br}$ and $[K^+]_{br}$ were determined by emission flame photometry in the micropunch samples obtained from all 8 animals between 2.5 and 6 hours after MCAO. Insets: coding of rat numbers by different symbols (top), and fit parameters (bottom). Dashed lines show 95% confidence limits.

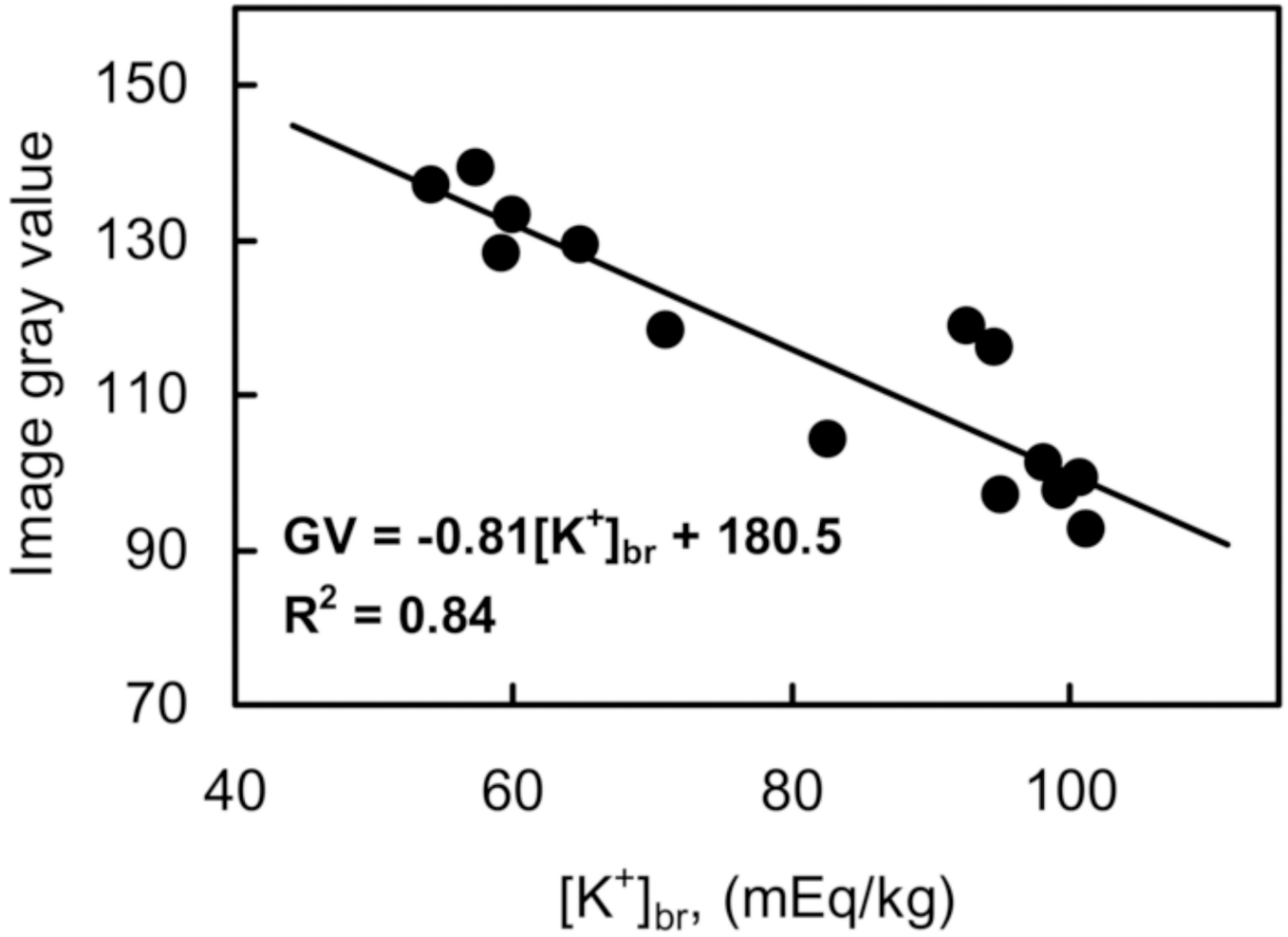

Figure 5.

Calibration of K^+ staining intensity by emission flame photometry. Horizontal axis: $[K^+]_{br}$ determined in punched samples by flame photometry. Vertical axis: digitized image intensity (GV, 8-bit gray value) averaged over ROIs precisely corresponding to the punch locations in immediately adjacent stained brain sections. A representative calibration curve for the rat #5 is shown. Calibration parameters for all rats are given in Table 2.

Table 1

Physiological variables at three phases of the protocol.

	MABP (mm Hg)	pH	$PaCO_2$ (mm Hg)	PaO_2 (mm Hg)
Before MRI	105 ± 9	7.38 ± 0.08	30 ± 10	100 ± 20
Start of ^{23}Na MRI	99 ± 7	7.25 ± 0.09	30 ± 14	120 ± 66
End of experiment	90 ± 12	7.26 ± 0.05	40 ± 10	100 ± 85

Mean ± SD, n = 8.

MABP, mean arterial blood pressure; pH, arterial blood pH; $PaCO_2$ and PaO_2, partial CO_2 and O_2 pressure in arterial blood, respectively.

Table 2

Sites of the fastest $[Na^+]_{br}$ growth and deepest $[K^+]_{br}$ depletion after MCAO.

Rat #	Ischemia model	T_d (h)[a]	Maximum slope ROI volume (mm^3)[b]	K^+ staining calibration parameters[c]	
				A	B (mEq/kg)
1	MCAT	4.9	_[d]	−0.55	164.6
2	suture	6.0	5.2	−0.58	171.8
3	suture	5.0	5.1	−0.76	173.8
4	suture	5.1	36.2	−0.96	174.3
5	suture	4.5	6.7	−0.81	180.5
6	suture	5.3	3.8	−0.48	149.0
7	suture	2.5	_[d]	−0.34	145.9
8	suture	5.3	_[d]	−0.46	163.2

[a] T_d, duration of the experiment after MCAO.

[b] Cutoff for the 3D isocontour ROIs of maximum ^{23}Na slope was set for each animal at 90% of their respective maximum slope.

[c] For the calibration equation $GV = A\,[K^+]_{br} + B$ (see Fig. 5).

[d] The ^{23}Na MRI protocol was not completed successfully in this animal.

Table 3

$[Na^+]_{br}$ and $[K^+]_{br}$ in different regions of ischemic brain.

Region		$[Na^+]_{br}$ (mEq/kg wet weight)		$[K^+]_{br}$ (mEq/kg wet weight)	
		Rostral	**Caudal**	**Rostral**	**Caudal**
1. Dorsal ischemic edge	ipsilateral	76±5	87±4	40±18	30±15
	contralateral	49±5	51±5	100±17	100±16
2. Central ischemic core	ipsilateral	68±6	73±4	70±17	80±13
	contralateral	49±4	51±4	100±13	113±9
3. Ventral ischemic edge	ipsilateral	100±4	95±6	50±19	40±16
	contralateral	54±4	60±3	100±19	110±13

$[Na^+]_{br}$ and $[K^+]_{br}$ (mean ± SD) were estimated by ^{23}Na MRI and histochemical K^+ staining, respectively, at the rostral (bregma −0.4 mm) and caudal (bregma −3 mm) coronal brain levels at 4.4 h after MCAO in rat #5. ROI placement is shown in Fig. 3. The SD values resulted from averaging over pixels within ROIs.

For every comparison of the ipsilateral and corresponding contralateral ROIs, $P < 0.05$.